

See discussions, stats, and author profiles for this publication at: <https://www.researchgate.net/publication/231710464>


A New Lamellar Morphology of a Hybrid Amorphous/Liquid Crystalline Block Copolymer Film

ARTICLE *in* MACROMOLECULES · APRIL 1999
Impact Factor: 5.8 · DOI: 10.1021/ma9812581

CITATIONS
22

READS
12

4 AUTHORS, INCLUDING:



D. Sentenac
European Gravitational Observatory

108 PUBLICATIONS 2,926 CITATIONS

SEE PROFILE

A New Lamellar Morphology of a Hybrid Amorphous/Liquid Crystalline Block Copolymer Film

D. Sentenac, A. L. Demirel, J. Lub, and W. H. de Jeu

FOM Institute for Atomic and Molecular Physics, Kruislaan 407, 1098 SJ Amsterdam, The Netherlands, and Philips Research Laboratories, Professor Holstlaan 4, 5656 AA Eindhoven, The Netherlands

Macromolecules[®]

Reprinted from
Volume 32, Number 10, Pages 3235–3240

A New Lamellar Morphology of a Hybrid Amorphous/Liquid Crystalline Block Copolymer Film

D. Sentenac,[†] A. L. Demirel,^{†,‡} J. Lub,[§] and W. H. de Jeu^{*,†}

FOM Institute for Atomic and Molecular Physics, Kruislaan 407,
1098 SJ Amsterdam, The Netherlands, and Philips Research Laboratories,
Professor Holstlaan 4, 5656 AA Eindhoven, The Netherlands

Received August 10, 1998; Revised Manuscript Received February 16, 1999

ABSTRACT: We study the morphology of a thin film made of a hybrid amorphous/side chain liquid crystalline diblock copolymer, in which the amorphous polymer is similar to the backbone of the liquid crystalline polymer. Microphase separation in the smectic A phase leads to a terraced film made of alternating amorphous and smectic layers, both parallel to the substrate. This new lamellar morphology differs from the bulk ordering where minimization of the block–block interfacial energy results in an orthogonal arrangement. We discuss the stability of such a lamellar structure in the film by considering the influence of the surface field on the internal diblock specific interactions.

Introduction

Block copolymers are an interesting and well-known variety of polymers. They possess the peculiar property of forming fairly well-defined mesoscopic structures, which makes them scientifically interesting as well as technologically attractive.¹

The most simple case is a diblock copolymer, composed of two polymers covalently bonded, of chemically distinct repeat units A and B. If A and B are incompatible, a microphase segregation can be obtained into, for example, spherical, cylindrical, or lamellar phases. The phase behavior depends on the relative volume fraction of A and B and on the magnitude of the product $\chi_{AB}N$, where χ_{AB} is the Flory–Huggins interaction parameter between the two polymers and N is the total degree of polymerization.² In the case of blocks of about equivalent size, the copolymer phase separates in a lamellar phase, with the scaling of the lamellar period being $\propto N^{2/3}$. This result comes from the balance between the enthalpic gain of unmixing A and B and the entropic cost of chain confinement within the layers.³ In thin films made of diblock copolymers, the interactions occurring at the air/film and film/substrate interfaces influence the microphase-separation process and can be used to control the orientation of the morphologies. For example, a preferential interaction of one of the blocks with the boundaries (“surfactant”-like behavior) will favor the formation of the lamellar phase on a macroscopic scale, with the lamellae of periodicity, L , parallel to the substrate.⁴ The resulting film thickness will belong to a discrete spectrum of allowed values d_n , where $d_n = (n + 1/2)L$, or $d_n = nL$, depending on the boundary conditions.^{4,5} Structural details of these morphologies have been investigated.^{6,7} The surface dynamics leading to the formation of such a quantized thickness has been compared to a 2D spinodal decomposition process.^{8,9}

The orientation of a macroscopic lamellar “stack” can be controlled further by using heterogeneous substrates.

Recently, lamellae orthogonal to laterally heterogeneous substrates were obtained by either considering the periodic variation of the preferential interactions of the block¹⁰ or by using laterally corrugated substrates.¹¹ Hybrid amorphous/liquid crystalline (LC) diblock copolymers offer an alternative to the use of heterogeneous substrates. If one of the polymers is a side chain LC polymer, i.e., the mesogens are attached laterally to the backbone, the phase structure will be driven both by the block incompatibility and the LC ordering.¹² An amorphous/smectic diblock can be considered to be an A(CB) triblock copolymer, where A denotes the amorphous polymer and C and B the backbone and mesogens of the LC polymer, respectively. The smectic layering can be considered to be a “nanophase” separation^{13,14} and the smectic to nematic or isotropic transition as the order–disorder transition. In general, one would expect that at temperatures in the smectic range, $\chi_{BC} \ll \chi_{AC}$ and $\chi_{BC} \ll \chi_{AB}$, which means that the microphase separation can be described effectively as a diblock system. In the bulk, the smectic layers are usually orthogonal to the lamellae and separate the microphase-segregated blocks. Similar structures with two length scales have recently been reached by using hydrogen-bonded diblock-amphiphile complexes.¹⁵ The ability of mesogenic units to homeotropically anchor onto a homogeneous substrate provides a new handle to manipulate the structure in thin films. In this situation, the diblock lamellae can be oriented perpendicular to the substrate.¹⁶

In this paper, we report on a new morphology of a thin hybrid amorphous/smectic block copolymer film for which the “diblock approximation” does not hold. As the backbone of the LC polymer is similar to the amorphous polymer, $\chi_{AC} \approx 0$, and $\chi_{BC} \approx \chi_{AB} \gg 0$. After annealing in the smectic A phase, we find an equilibrium structure with both of the smectic and amorphous layers parallel to the substrate. This situation differs from the bulk, where the lamellae are found to be orthogonal to the smectic layers.¹⁷ In the next section, we describe the systems studied and the experimental techniques used to collect complementary real and reciprocal space information, i.e., atomic force microscopy (AFM) and specular X-ray reflectivity (SXR), respectively. The

* Corresponding author.

[†] FOM Institute for Atomic and Molecular Physics.

[‡] Permanent address: Chemistry Department, Koc University, Cayir Cad., Istinye, 80860 Istanbul, Turkey.

[§] Phillips Research Laboratories.

Table 1. Bulk Characteristics of the Polymers¹⁷

polymer	M_n	polydispersity	Φ_{PIBVE}	phase behavior (°C)
homopolymer	8700	1.40		g (9), SmC* (45), SmA (75), I
diblock	9600	1.26	0.33	g (-19), g (11), SmC* (44), SmA (67), I

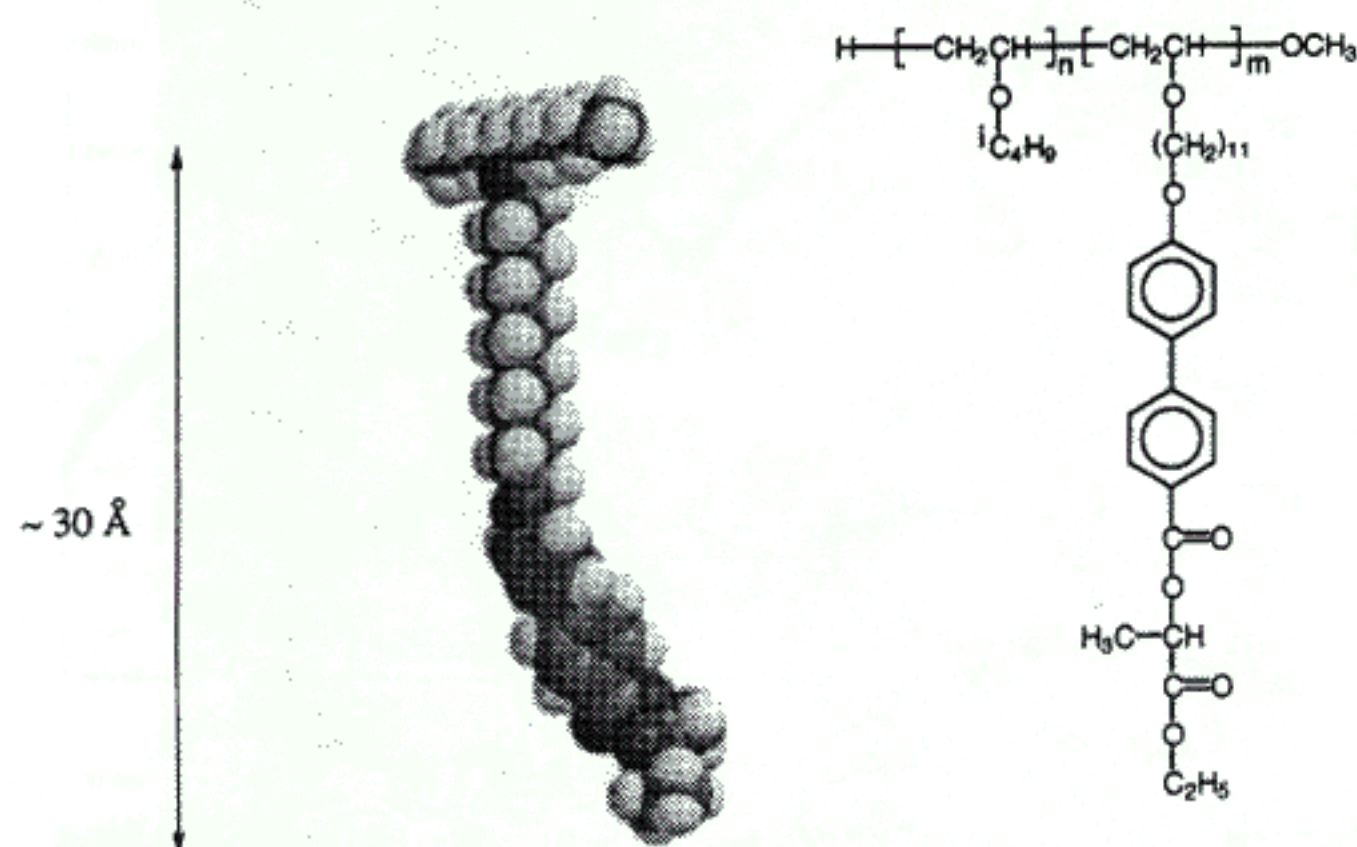


Figure 1. Structure and molecular model of the liquid crystalline diblock copolymer investigated.

results are presented and discussed in Results and Discussion.

Experimental Section

The polymeric materials under consideration have been synthesized by a cationic polymerization at Philips Research Laboratories.¹⁷ The diblock copolymer consists of an amorphous polymer A which consists of a poly(isobutyl vinyl ether) (PIBVE), chemically linked to a side chain LC block (A'B). The LC polymer is composed of a poly(vinyl ether) backbone (A') to which mesogenic units (B) are laterally attached via an alkyl spacer (see Figure 1). The bulk characteristics of the polymers as given in Omenat et al.¹⁷ are summarized in Table 1. For the diblock, two glass transitions have been detected in DSC, which is direct proof of the immiscibility of the blocks. The backbones of the two different polymers consist of the same vinyl ether monomer. Therefore, the system cannot be described as a conventional diblock, because the amorphous block is only incompatible with part of the LC block. Hence, we can expect the LC properties to be dominant. To describe the phase separation of the present diblock system, we can separate the interaction parameter into $\chi_{AA'}$, χ_{AB} , and $\chi_{A'B}$ contributions with $\chi_{AA'} \approx 0$ and $\chi_{AB} \approx \chi_{A'B} \gg 0$.

The length of the stretched mesogenic unit is ~ 30 Å. In the SmC* and SmA phases, the diffraction pattern of the bulk diblock shows the existence of a smectic periodicity of approximately 31–33 Å orthogonal to the lamellar diblock period of 107 Å.¹⁷ In the bulk smectic phases, the mesogens form interdigitated layers.

Thin films were obtained by spin-coating from a chlorobenzene solution onto quartz substrates. The initial thickness of the films depends on the polymer concentration and the spinning velocity. The films were annealed in the smectic A phase and then quenched to room temperature ($20 \pm 1^\circ\text{C}$ in the SmC* phase) for further analysis. We studied a thin film of a homopolymer solution at 7.3 mg/mL, spin-coated at 2000 rpm, and annealed at $T = 70^\circ\text{C}$ during 60 h, as well as a thin film of a diblock solution at 15.6 mg/mL, spin-coated at 2000 rpm, and annealed at $T = 63^\circ\text{C}$ during 60 h.

Direct images of the surface of the thin films were obtained with an AFM apparatus (Solver SFM, NT-MDT, Zelenograd, Moscow) in the semicontact mode. Standard probes, with ~ 10 nm radii type and a cantilever resonant frequency of ~ 300 kHz, were used to scan the samples, which were kept in a dry nitrogen atmosphere to limit water condensation. Because of the very slow evolution dynamics at room temperature, the AFM topographies show no change during successive scans.

SXR measurements were performed using the Cu K α line (wavelength $\lambda = 1.54$ Å) from a rotating anode generator and

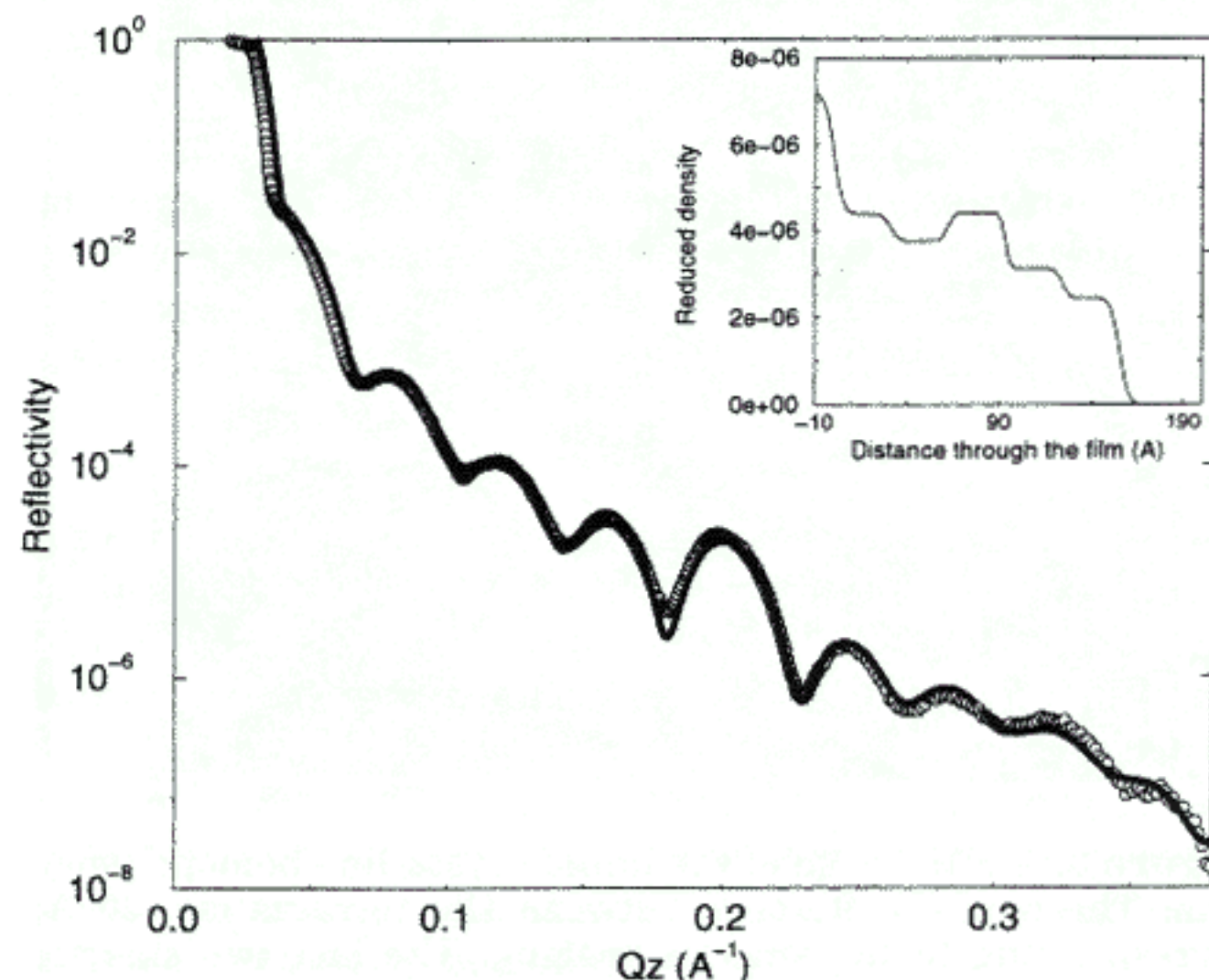


Figure 2. X-ray reflectivity curve of the liquid crystalline homopolymer film (circles) with a fit using the density profile depicted in the inset (solid line).

the triple-axis reflectometer described in Mol et al.¹⁸ The incident beam was monochromatized and focused in the direction perpendicular to the scattering plane with a bent graphite (002) crystal. In reciprocal space, the specular scans probe the scattered intensity along q_z , the z axis being in the direction perpendicular to the film. The analysis of the specular reflectivity profiles is performed rigorously through the use of an optical formalism valid at all angles,¹⁹ convoluted with the experimental resolution, and assumed to obey Gaussian statistics. The film is described by a succession of homogeneous slabs, each of them characterized by three parameters: thickness, electron density, and interfacial roughness σ . The electron density is related to the refractive index via the relation $\rho = 2\pi\delta/(\lambda^2 r_e)$, where r_e is the classic radius of electron and δ is the so-called reduced density. The incoming divergence, as defined by the presample slit widths was set to 0.064° , corresponding to an in-plane resolution $\Delta q_z = 7.4 \times 10^{-3} \text{ Å}^{-1}$.

Results and Discussion

Liquid Crystalline Homopolymer. To get preliminary information about the LC behavior of the diblock, it is important to study first the ordering in homopolymer films. Figure 2 shows the X-ray reflectivity curve of such a film with a thickness of about 150 Å. The reflectivity exhibits a clear Bragg peak at $q_z = 0.2 \text{ Å}^{-1}$, corresponding to smectic ordering with a period of 31 Å. Hence, the mesogenic units are organized in smectic layers parallel to the substrate. The best fit of the reflectivity can be achieved by using a unit cell of size 31 Å, smeared by interfacial roughnesses varying from 3 to 5.5 Å. The smectic period is equal to the stretched size of the side groups, indicating that these are homeotropically oriented. The electron density profile through the film is shown in the inset of Figure 2. As can be seen there, the density profile contains five layers of unequal densities, which suggests that the mesogenic units are nonuniformly distributed inside the film. Assuming a structure of interdigitated side groups, the irregular density profile can be partly explained by assuming relatively strong anchoring of the mesogenic units onto the substrate. This would induce a preferred

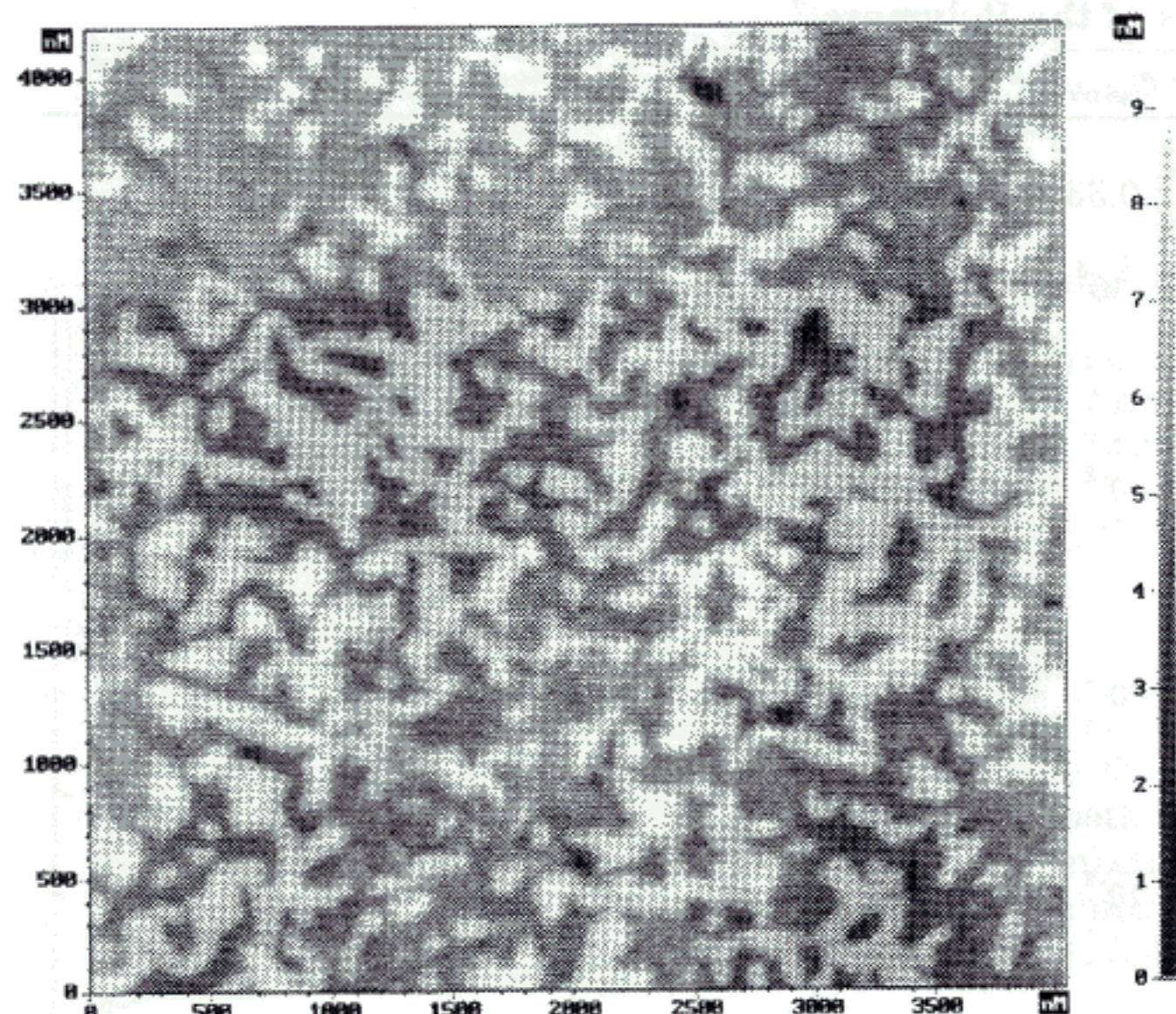


Figure 3. AFM image of the liquid crystalline homopolymer film. The height difference between the terraces is ~ 30 Å, corresponding to the smectic spacing. The last two smectic layers are incomplete.

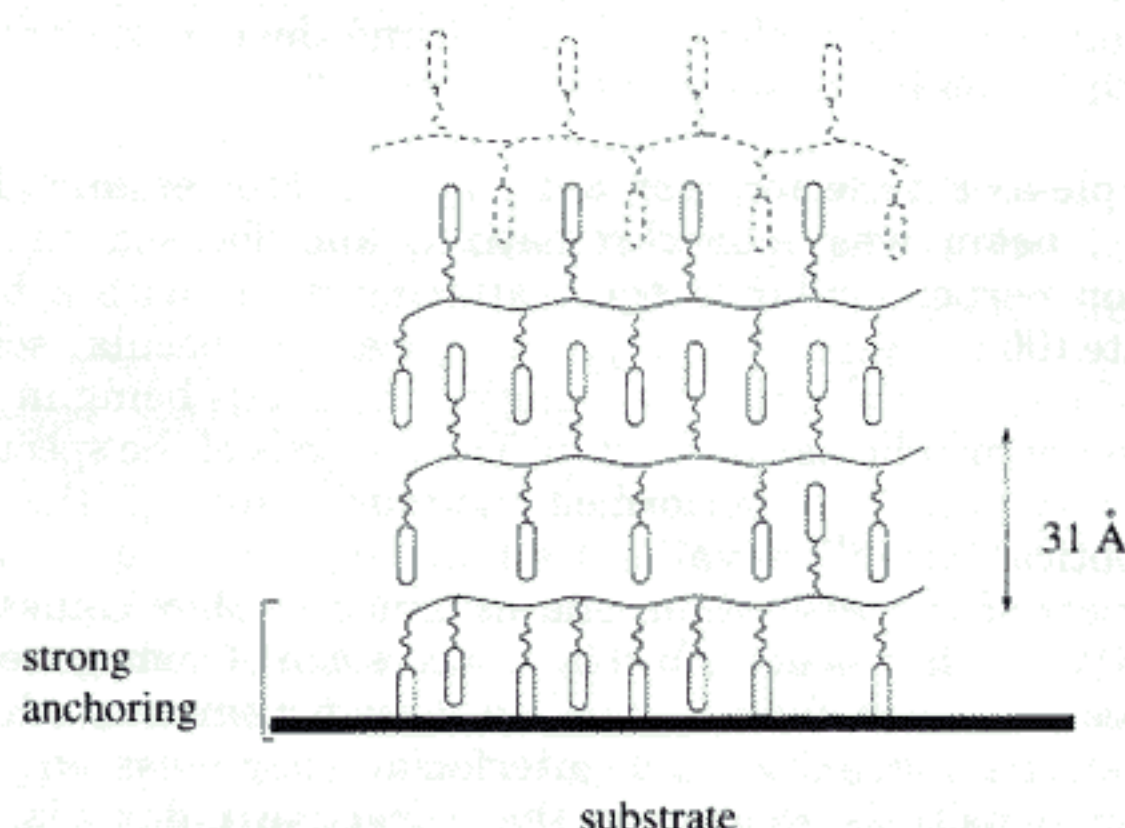


Figure 4. Microscopic model proposed for the liquid crystalline homopolymer film. The last two layers are incomplete because of the lack of material left to cover the film surface (see AFM image in Figure 3). The density difference detected between the first two layers close to the substrate may be due to the preferential mesogens/substrate interaction.

orientation of the mesogenic units connected to the backbone closest to the surface toward the surface ("down"). This, in turn, will give a relative shortage of the mesogenic units oriented "up" in the second layer, necessarily followed by a subsequent increase in the next one. Furthermore, the last two layers are not filled because of a lack of material, as demonstrated by AFM imaging (see Figure 3). This qualitatively explains the decreasing density of the last two layers close to the air/film interface. A comprehensive microscopic scheme of the morphology is depicted in Figure 4. Note that this model assumes that two neighboring mesogenic groups point in the same direction. In fact, the space available for such a situation is severely restricted by a single methyl group in the backbone that separates them. However, the relatively long size of the spacers connecting the mesogens with the main chain can still provide the necessary flexibility to obtain a variety of packing configurations in 3D.

A preferential interaction between the boundary layer and the substrate has been evidenced from a sample annealed in the isotropic phase ($T = 80$ °C) during 50

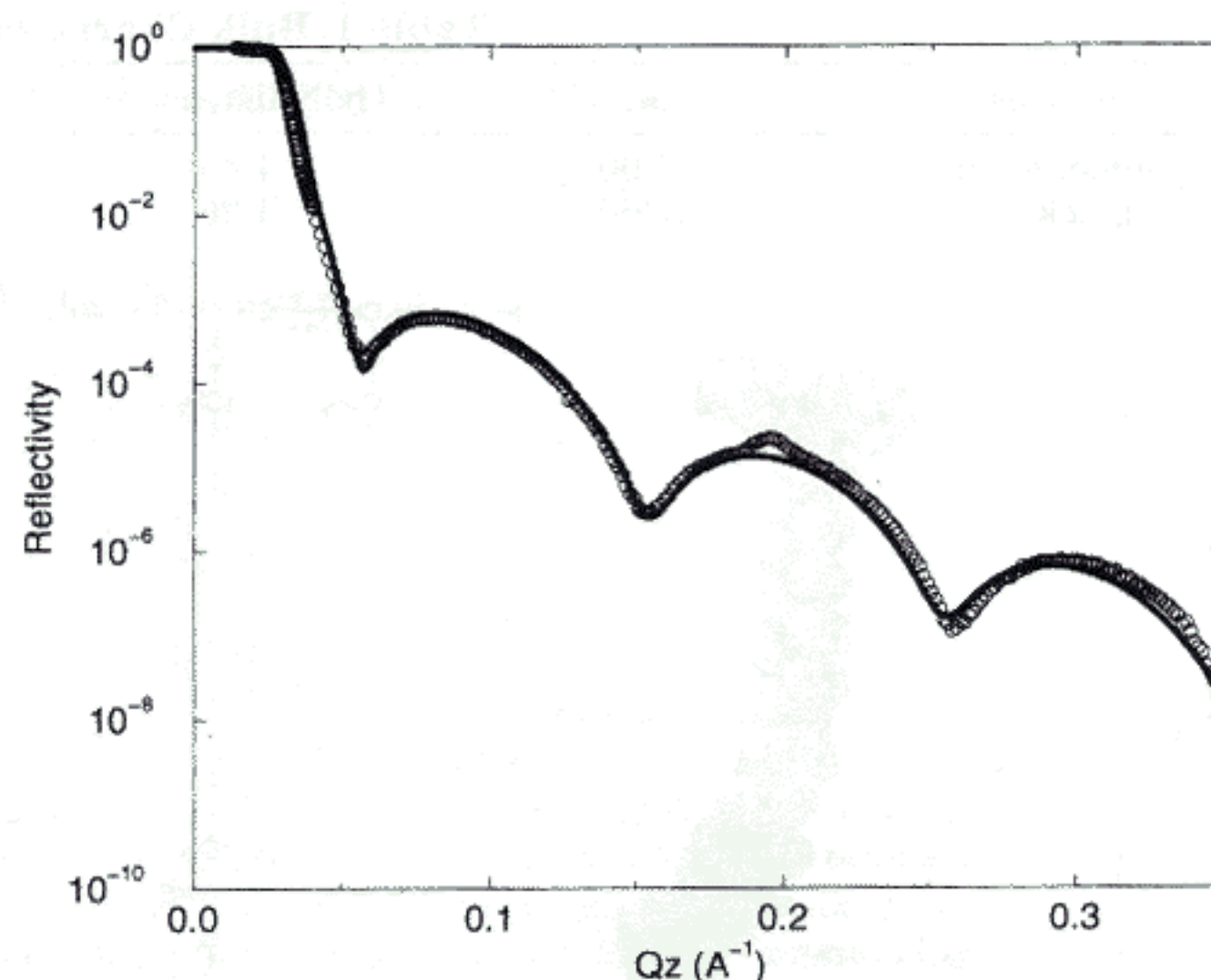


Figure 5. X-ray reflectivity curve of the liquid crystalline homopolymer film after annealing in the isotropic phase at $T = 80$ °C (circles). A 62 Å thick bilayer remains strongly anchored to the glass substrate (fit represented by the solid line). A small bump at $q_z = 0.2$ Å $^{-1}$ denotes a smectic layering inside the dewetted droplets.

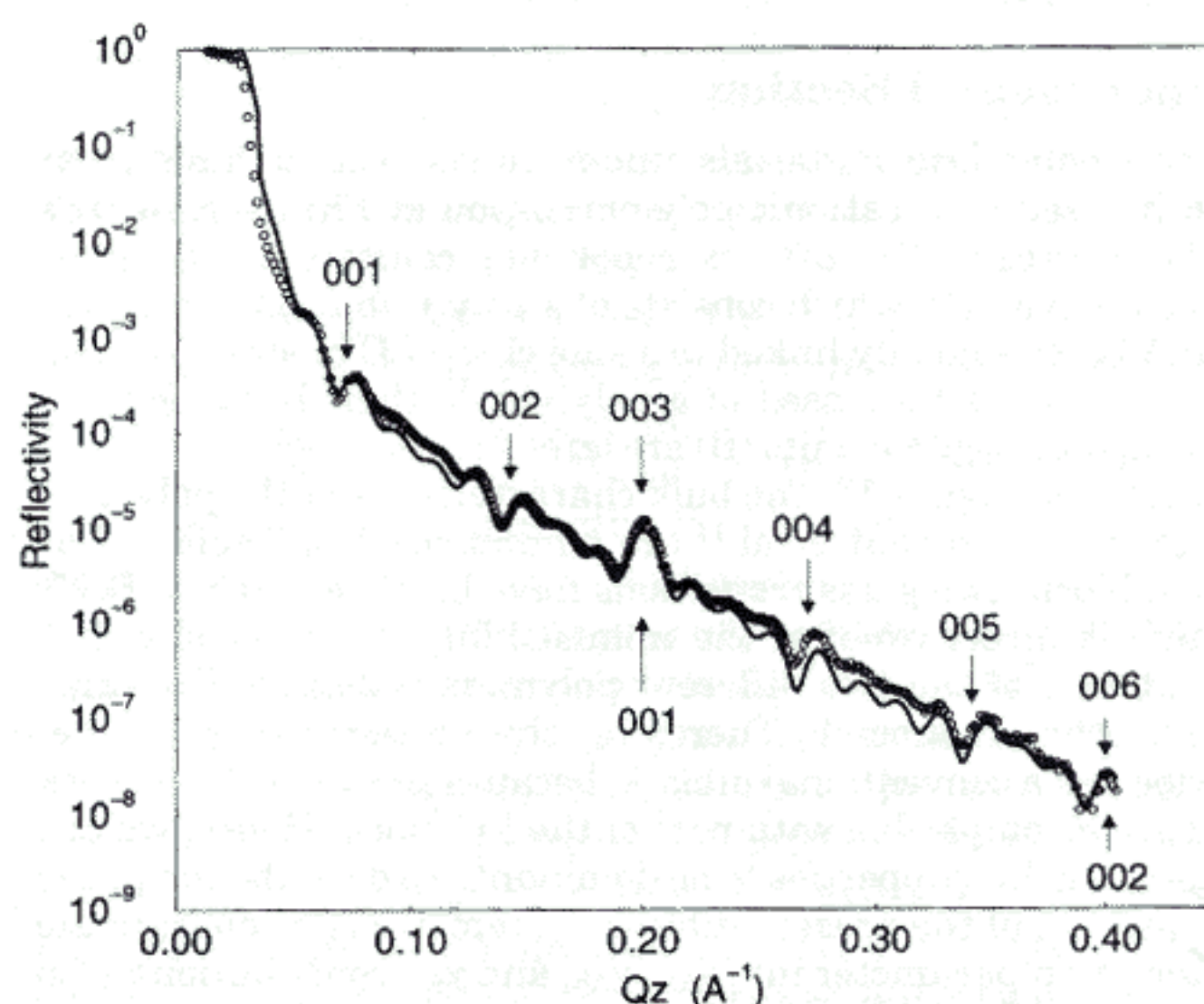


Figure 6. X-ray reflectivity of the diblock film after annealing in the SmA phase at $T = 63$ °C (circles) and the possible fitting curve (solid line) discussed in the text. The Bragg positions (00 l) of the diblock periodicity (above the curve) and of the smectic spacing (below the curve) are indicated.

h. The resulting SXR curve is shown in Figure 5. It appears that the film has dewetted the substrate, except from a homogeneous 62 Å thick layer, corresponding to exactly two smectic layers. Only the anchored molecules remain on the substrate in the isotropic phase, which shows qualitatively the relative importance of this interaction. In addition, one can notice a small bump on top of the Kiessig fringes at $q_z = 0.2$ Å $^{-1}$, which indicates a persistent smectic ordering within droplets on top of the surface layer. The existence of such smectic boundary layers in the isotropic phase has been reported for several LC systems and is understood as a pretransitional surface ordering phenomenon.²⁰

Diblock Copolymer. The SXR curve corresponding to a diblock film with a thickness of about 360 Å is shown in Figure 6. In addition to the Kiessig fringes leading to this thickness, one can observe additional periodicities. Bragg-like features at $q_z \approx 0.07$ Å $^{-1}$, with

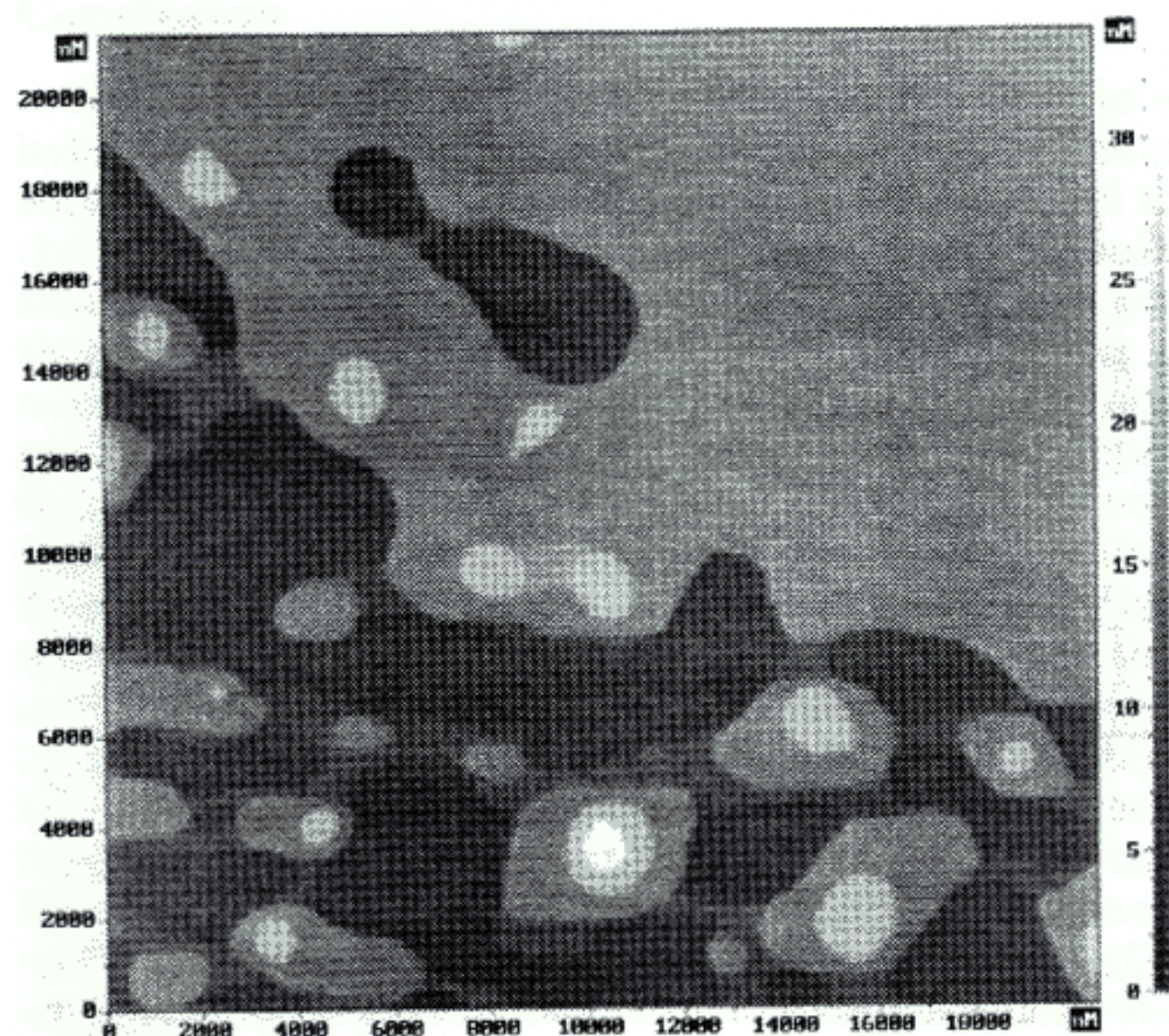


Figure 7. AFM image of the diblock film. The height difference between the terraces is ~ 90 Å. Adjacent to the terraces are dewetting layers ~ 30 Å thick.

five higher orders indicates the presence of a lamellar period of thickness of ~ 90 Å, with a long-range spatial order. This lamellar period is smaller than the bulk lamellar period (107 Å¹⁷). Moreover, one can see that the height of the third order, at $q_z = 0.2$ Å⁻¹ is much higher than the other Bragg features. In fact, it is located at the same position as the first-order Bragg peak related to the smectic layering (thickness ≈ 30 Å) parallel to the substrate, as already observed for the homopolymer film. Evidently, this is the natural way to explain the difference in height between the Bragg position at $q_z = 0.2$ Å⁻¹ and the other ones. It leads to a new lamellar morphology in the diblock film, with both smectic and amorphous layers parallel to the substrate.

Fits to the reflectivity data indicate that the density profile through the film is composed of 12 layers of thickness of about 30 Å $\pm 15\%$, and that interfacial roughnesses vary between 5 and 10 Å. Moreover, the density profile decreases monotonically from the substrate to the air/film interface and is unrealistically low for most of the layers.

More insight about the diblock film structure is provided by the AFM data. Figure 7 shows an AFM image of a diblock film, prepared under identical conditions. One can see terraces, the area of which decreases monotonically from the substrate to the air. The terraces are all ~ 90 Å thick and have a roughness of ~ 10 Å. Hence, the AFM image confirms the presence of lamellae parallel to the substrate.

The decrease in area of the terraces on top of each other, as clearly visible on a local scale in Figure 7, is consistent with the monotonically decreasing density of the slabs in the SXR model. Reasonable fits of the SXR data can be obtained by averaging individually the reflectivity of four different films of thicknesses of 1 to 4 lamellae and realistic densities in the range $3 \leq d \times 10^6 \leq 4$. Thus, the unrealistically low densities described above can be attributed to an averaging over the various terraces within the illuminated area.

We further notice in Figure 7 the presence of instabilities during the microphase separation, which hinder the formation of the lamellae on a large in-plane scale. The AFM picture shows intermediate layers of ~ 30 Å

thickness between adjacent terraces. These layers are dewetting the underneath terrace, as indicated by their irregular contours. In fact, during the phase segregation process, islands and depressions of ~ 30 Å thickness are successively formed. As a result, most of the 30 Å thick layers at the air/film interface are unstable, leaving a few stable terraces of ~ 90 Å thickness. The fact that the areas of the terraces decrease from bottom to top suggests that the organization of the lamellar structure starts from the substrate level and that interactions at the substrate level are the starting point for the development of the parallel smectic/lamellar block morphology.

The lamellar period of ~ 90 Å must be composed of a smectic block of ~ 60 Å, and an amorphous block of ~ 30 Å, to be consistent with the bulk volume fraction of the blocks ($\Phi_{\text{PIBVE}} = 0.33$). Generally, such a parallel lamellar structure will be configurationally frustrated, because the smectic block size, as obtained by scaling the lamellar diblock period, may be incommensurate with the smectic periodicity.¹⁶ However, for the present volume fractions, the smectic block size corresponds to twice the smectic periodicity.

Several lamellar morphologies are possible with parallel lamellae and smectic layers. Various combinations of alternating amorphous blocks and an integral number of smectic layers can be obtained, with the mesogens oriented up and down with respect to the backbone. However, for neither of these cases, a lamellar period of ~ 90 Å can be constructed. Moreover, this situation leads to an unfavorable contact area between A and B components. We recall that the main segregation is due to the unfavorable χ_{AB} and $\chi_{A'B}$, between the amorphous polymer A and the mesogenic units B and between the backbone A' and its side groups B, respectively. The above considerations bring us to another possibility of a radically different mesogens packing within the smectic layers. Contrary to the homopolymer film, the mesogenic units are assumed to be densely packed and all pointing in the same direction (Figure 8b). By alternating with the smectic layers, the PIBVE block will form the second sublayer. As the side groups point in the same direction, the polymer A and backbone A' face each other in a favorable way, because they are practically of the same chemical composition ($\chi_{AA'} \approx 0$). In addition, phase segregation between the A and A' components and the B component is ensured. In this situation, the smectic and amorphous blocks sizes correspond to ~ 60 and ~ 30 Å, respectively, in agreement with the lamellar period. Unfortunately, the SXR reflectivity of the diblock does not confirm the unidirectional mesogens conformation, as the film inhomogeneities (terraced structure) prevent us from making a more quantitative analysis of the densities.

Nevertheless, in contrast to the bulk and homopolymer situations, a unidirectional conformation of the mesogens seems the only way that allows a combination of the phase-separated structure and the smectic LC/substrate preferential interactions. The difference in stability between the bulk structure of Figure 5a and the film structure of Figure 8b can be interpreted as follows. The free energetic contributions of the smectic ordering in the bulk and in the film are different because of dissimilar mesogens packing configurations. The interdigitated smectic ordering of Figure 8a is the natural morphology, as shown by the homopolymer film analysis, and could be more favorable than that of

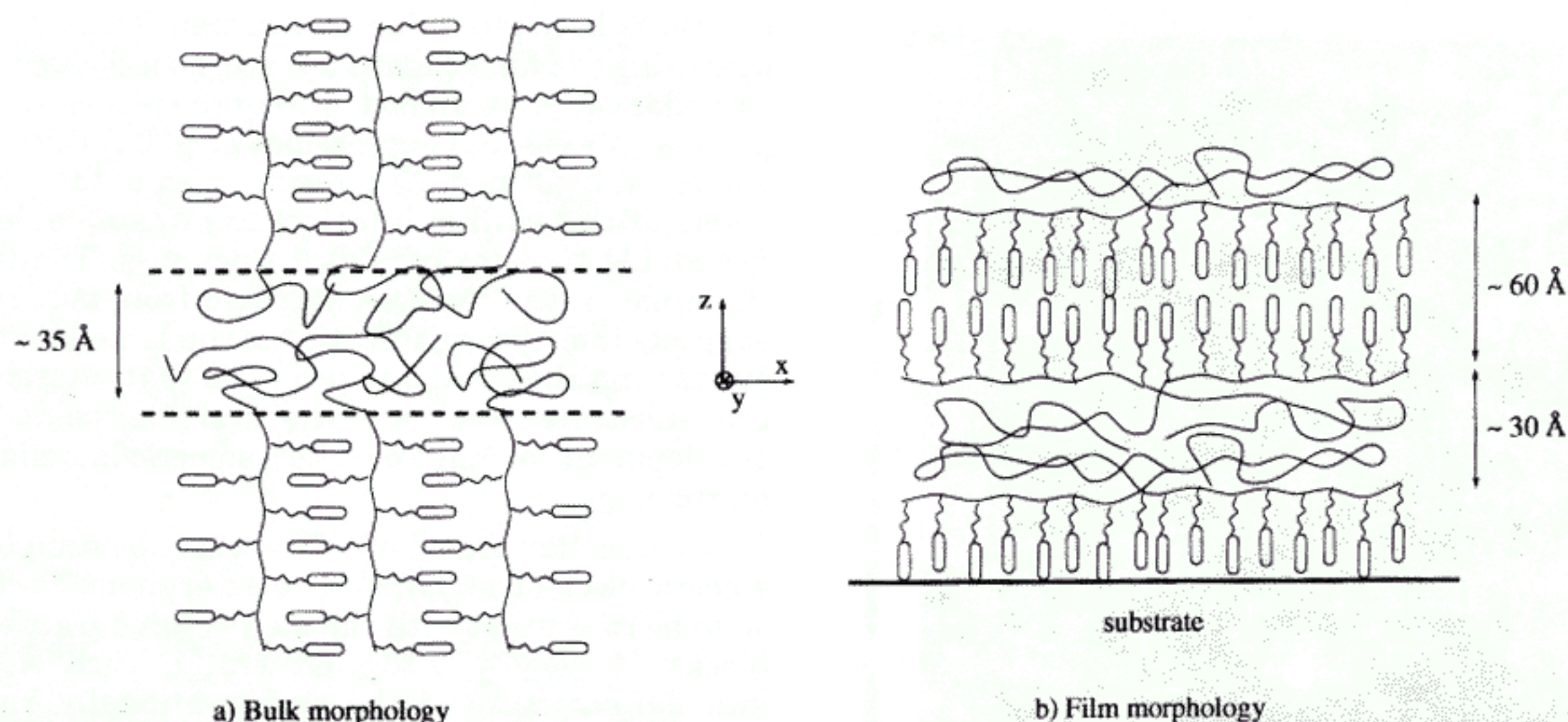


Figure 8. Microscopic models of the bulk orthogonal lamellar morphology and the film parallel lamellar morphology. (a) The bulk perpendicular morphology presents an excess interfacial free energy due to the mixing and confinement of incompatible components in the transition layer (dashed lines). (b) The film parallel lamellar morphology here combines segregated incompatibles parts and strong mesogens/substrate interactions. This model leads to an excess chain stretching of the amorphous polymer along the block interface and an excess entropic cost due to the confinements mesogens within the smectic layers.

Figure 8b, which supposes a relatively strong confinement of the mesogens. However, two other contributions to the free energy have to be considered. In the bulk (see Figure 8a), the block-block transition layer contributes to an unfavorable free energy of mixing of the A and B components. The interfacial area per polymer scales approximately with the smectic period. Therefore, the excess enthalpy of mixing can be approximated by $kT\chi_{AB}N^{\text{mix}}_A$, where N^{mix}_A represents the number of A monomers in the transition layer. The amorphous polymer possesses $N_A \approx 30$ units of size $a \approx 3$ Å, and the LC polymer has ~ 15 mesogens of size 30 Å. The smectic period being ~ 30 Å, we roughly estimate as an average value $N^{\text{mix}}_A \approx 10$ units in contact with one mesogen. The minimal value for χ_{AB} to obtain the segregation regime is given by $\chi_{AB}N \gtrsim 10$,² where N is the total degree of polymerization assuming that units of both polymers are of equal size. Taking the size of both polymer units into account, we estimate $\chi_{AB} \approx 0.1$ as a minimum value. We find an excess interfacial enthalpic cost of about kT per copolymer. The free energy of mixing of the transition layer may be further increased by the loss of entropy connected with the confinement of the junction points. This entropic contribution can be written as $\sim kT \ln(l_t/L)$, where l_t is the transition layer thickness, and $L \approx 90$ Å is the lamellar period. We estimate $l_t \approx 10$ Å from the X-ray reflectivity interfacial roughness data, which leads to an entropic loss per copolymer of about $2kT$. In the film morphology (see Figure 8b), these contributions vanish, because the amorphous polymer avoids all contacts with the mesogens of the smectic block ($\chi_{AA'} \approx 0$). We conclude that the excess interfacial free energetic change from the bulk to the film configuration is about $-3kT$ per copolymer.

A second aspect to analyze for both cases is the packing configuration of the amorphous block. The elastic entropy change of the amorphous chain between the bulk and film morphologies can be expressed qualitatively as $\sim kT(R_f^2 - R_b^2)/(a^2N_A)$ where $R^2 = R_x^2 + R_y^2 + R_z^2$ denotes the squared end-to-end distance of a single chain in the bulk (b) and in the film (f), respectively. Assuming that the chain sizes and the layers

spacings are linearly related, we can estimate numerical values for R_b and R_f . In the bulk, let us choose the x -direction normal to the smectic layers and the z -direction normal to the block interface (see Figure 8a). In the direction normal to the interface, $R_{bz} \approx 35$ Å scales with the amorphous block period.¹⁷ Normal to the smectic layers, $R_{bx} \approx 30$ Å scales with the smectic period. From the bulk diffraction pattern,¹⁷ the mesogen-mesogen distance is found to be ~ 5 Å, which we take as R_{by} . In the film, $R_{fz} \approx 30$ Å, scales with the amorphous period. Contrary to the bulk, the (Ox) direction can no longer be distinguished from the (Oy) one (the smectic and lamellar directors are parallel). However, the LC polymer's backbone is expected to be stretched because of the packing restrictions due to the unidirectional mesogens orientation. Let us choose (Ox) in the direction along the backbone (see Figure 8a). R_{fx} may be slightly larger than in the bulk, as it scales with the length of the stretched backbone: $R_{fx} \approx 38$ Å. We may expect that R_{fy} is smaller than in the bulk, because of the strong confinement of the mesogens, say, $R_{fy} \approx 4-5$ Å. We find an elastic entropy change from the bulk to the film morphology smaller than kT per copolymer.

Without considering the LC phase free energetic change, from the above calculations, the morphology of Figure 8b appears slightly more stable than that of Figure 8a. However, from the AFM data, the film lamellar morphology appears unstable (dewetting layers and terraced film). Hence, it may be due to the additional entropic penalty coming from the packing restrictions of the mesogens within the smectic layers. As mentioned above, the area of the terraces decreases from the substrate to the air as direct evidence of the strong surface-induced nature of the parallel lamellar morphology in the film. We believe that the parallel lamellar structure of Figure 8b originates from the strong interaction between the mesogenic units and the substrate. The favorable internal diblock interactions will maintain the parallel lamellar structure, as long as the entropic cost due to the confinement of mesogens within the smectic layers is compensated for by the mesogens/substrate enthalpic bonus.

Conclusion

We have evidenced a new lamellar morphology in a hybrid amorphous/smectic LC diblock copolymer film where both smectic layers and lamellae are parallel to the substrate. This morphology differs from the bulk situation where smectic layers and lamellae are orthogonal. The lamellar morphology in the film has a period of ~ 90 Å. To accommodate this period, a confined packing of the mesogens, pointing into the same direction, must be assumed, contrary to the bulklike interdigitated packing observed in the LC homopolymer film. The occurrence of this particular diblock lamellar morphology is attributed to the similarity between the amorphous polymer A and the LC polymer's backbone A', combined with the strong mesogens/substrate interactions. The surface-induced orientation of mesogens favors A and A' component interactions through the film, leading to the phase-segregated lamellar morphology with parallel lamellae and smectic layers. We interpret the stability behavior of the film lamellar morphology away from the substrate surface as resulting from the subtle balance between the mesogens/substrate enthalpic bonus and the entropic penalty due to the mesogens confinement within the smectic layers.

Acknowledgment. We thank Dr. A. Omenat (presently at the University of Zaragoza) for preparing the polymers. We thank Andrea Fera for valuable discussions. This work is part of the research program of the "Stichting voor Fundamenteel Onderzoek der Materie" (Foundation for the Fundamental Research of Matter, FOM), which is financially supported by the "Nederlandse Organisatie voor Wetenschappelijk Onderzoek" (Netherlands Organization for the Advancement of Research, NWO). D.S. acknowledges support from the TMR-Program of the European Union (ERBFMCT 9828877).

References and Notes

- (1) Park, M.; Harrison, C.; Chaikin, P. M.; Register, R. A.; Adamson, D. H. *Science* **1997**, *276*, 1401.
- (2) For example, see: Bates, F. S.; Frederickson, G. H. *Annu. Rev. Phys. Chem.* **1990**, *41*, 525 and references therein.
- (3) Strobl, G. *The Physics of Polymers*; Springer, Berlin, 1996.
- (4) Russell, T. P.; Coulon, G.; Deline, V. R.; Miller, D. C. *Macromolecules* **1989**, *22*, 4600.
- (5) Coulon, G.; Russell, T. P.; Deline, V. R.; Green, P. F. *Macromolecules* **1989**, *22*, 2581.
- (6) Coulon, G.; Collin, B.; Ausserre, D.; Chatenay, D.; Russell, T. P. *J. Phys. (Paris)* **1990**, *51*, 2801.
- (7) Maaloum, M.; Ausserre, D.; Chatenay, D.; Coulon, G.; Gallot, Y. *Phys. Rev. Lett.* **1992**, *68*, 1575.
- (8) Maaloum, M.; Ausserre, D.; Chatenay, D.; Gallot, Y. *Phys. Rev. Lett.* **1993**, *70*, 2577.
- (9) Joly, S.; Raquois, A.; Paris, F.; Hamdoun, B.; Auvray, L.; Ausserre, D.; Gallot, Y. *Phys. Rev. Lett.* **1996**, *77* (21), 4394.
- (10) Rockford, L.; Liu, Y.; Mauskay, P.; Russell, T. P.; Yoon, M.; Mochrie, S. G. *J. Phys. Rev. Lett.* **1999**, *82* (12), 2602.
- (11) Fasolka, M. J.; Harris, D. J.; Yoon, M.; Mochrie, S. G. *J. Phys. Rev. Lett.* **1997**, *79* (16), 3018.
- (12) Fischer, H.; Poser, S.; Arnold, M.; Frank, W. *Macromolecules* **1994**, *27*, 7133. Mao, G.; Wang, J.; Clingman, S. R.; Ober, C. K.; Chen, J. T.; Thomas, E. *Macromolecules* **1997**, *30*, 2556. Galli, G.; Chiellini, E.; Laus, M.; Ferri, D.; Wolff, D.; Springer, J. *Macromolecules* **1997**, *30*, 3417. Bohnert, R.; Finkelmann, H. *Macromol. Chem. Phys.* **1994**, *195*, 689. Sanger, J.; Gronski, W.; Maas, S.; Stuhn, B.; Heck, B. *Macromolecules* **1997**, *30*, 6783.
- (13) Guillon, D.; Poeti, G.; Skoulios, A.; Fanelli, E. *J. Phys. Lett. (Paris)* **1983**, *44*, L-491.
- (14) Diele, S.; Oelsner, S.; Kuschel, F.; Hisgen, B.; Ringsdorf, H.; Zentel, R. *Macromol. Chem. Phys.* **1987**, *188*, 1993.
- (15) Ruokolainen, J.; Makinen, R.; Torkkeli, M.; Makela, T.; Serimaa, R.; ten Brinke, G.; Ikkala, O. *Science* **1998**, *280*, 557.
- (16) Wong, G. C. L.; Commandeur, J.; Fischer, H.; de Jeu, W. H. *Phys. Rev. Lett.* **1996**, *77*, 5221.
- (17) Omenat, A.; Hikmet, R. A. M.; Lub, J.; van der Sluis, P. *Macromolecules* **1996**, *29*, 6730.
- (18) Mol, E. A. L.; Shindler, J. D.; Shalaginov, A. N.; de Jeu, W. H. *Phys. Rev. E* **1996**, *54*, 536.
- (19) Parrat, L. G. *Phys. Rev.* **1954**, *95*, 359.
- (20) Elben, H.; Strobl, G. *Macromolecules* **1993**, *26*, 1013.

MA9812581